Mixed Rossby–Gravity Waves and Western Pacific Tropical Cyclogenesis. Part I: Synoptic Evolution

MICHAEL DICKINSON AND JOHN MOLINARI

Department of Earth and Atmospheric Sciences, University at Albany, State University of New York, Albany, New York

(Manuscript received 2 August 2001, in final form 4 February 2002)

ABSTRACT

A large-amplitude mixed Rossby–gravity wave packet is identified in the western Pacific using 6–10-day bandpass-filtered winds. Individual disturbances of 2300–3000-km wavelength propagated westward as the packet moved slowly eastward. The packet first appeared, and subsequently amplified, within a region of active convection associated with the Madden–Julian oscillation (MJO), which was isolated by low-pass-filtered outgoing longwave radiation. The packet lasted about 5 weeks, then rapidly dispersed as the active MJO moved away from it to the east.

West of 150°E, individual disturbances within the packet turned northwestward away from the equator, indicating an apparent transition from mixed Rossby–gravity waves to off-equatorial tropical depression (TD)-type disturbances. Cyclones filled with cloud and anticyclones cleared during the transition. Nevertheless, convective structure consistent with mixed Rossby–gravity waves remained outside the circulation centers, and three tropical cyclones formed on the edges of three consecutive cyclonic gyres as they moved off the equator. Although the expected Rossby–Kelvin wave structure was present in the background winds within the active MJO, tropical cyclone genesis did not occur within the trailing Rossby gyres, but 2500 km to the west and north.

This case study provides evidence that equatorial modes, under the right conditions, can supply precursor disturbances for repeated formation of tropical cyclones. It is argued based on previous work in the literature that this sequence of events is not uncommon.

1. Introduction

Three broad classes of westward-propagating lower-tropospheric disturbances with periods between 3 and 10 days are found in the Tropics and subtropics: off-equatorial easterly waves, now often called tropical depression (TD)-type disturbances, with predominant periods of 3–6 days; mixed Rossby–gravity (MRG) waves, also most common in the 3–6-day period; and a third type of disturbance with a 6–10-day period that has not been identified with a specific wave type.

TD-type disturbances show clearly in the outgoing longwave radiation (OLR) spectrum during Northern Hemisphere summer (Wheeler and Kiladis 1999) with horizontal scales in the range of 3000–6000 km. These waves have been studied in the central and western Pacific by Reed and Recker (1971, hereafter RR71) using rawinsondes located between 7° and 11°N. Their mean wavelength was 3800 km and westward phase speed was 9 m s^{-1}. The disturbance tilt changed from the central to the western Pacific, from a small eastward tilt near 170°E to a strong westward tilt near 135°E. The latter represented a downshear tilt in the presence of strong easterly vertical wind shear. Maximum precipitation occurred within and downshear of the cyclonic disturbances.

Lower-tropospheric MRG waves with 3–6-day periods have been identified in the central Pacific. These had wavelengths of 7000–10 000 km, a westward phase speed of 15–20 m s^{-1}, and an eastward group speed of roughly 5 m s^{-1} (Liebmann and Hendon 1990; Takayabu and Nitta 1993; Dunkerton and Baldwin 1995). Liebmann and Hendon (1990) noted that MRG waves in the western Pacific had much shorter wavelengths and slower westward phase speeds than in the central Pacific. Takayabu and Nitta (1993) identified a storm track using 3–5-day bandpass-filtered 850-hPa meridional wind. Variance maxima in this field extended along the equator from near the date line to 160°E, then northwestward toward the Philippines. Convection in the disturbances evolved from a structure consistent with the linear MRG mode convergence field (Hendon 1986; Liebmann and Hendon 1990) in the central Pacific to filling the center of counterclockwise gyres as the disturbances turned northward away from the equator in the western Pacific (Takayabu and Nitta 1993; Dunkerton and Baldwin 1995). This apparent transition from MRG to TD-type disturbances occurred in the vicinity of 150°–160°E.

Corresponding author address: Michael Dickinson, Department of Earth and Atmospheric Sciences, University at Albany, State University of New York, Albany, NY 12222.
E-mail: mjd@atmos.albany.edu

Hendon and Liebmann (1991) showed a maximum in the 850-hPa meridional wind power in the 4.5-day band that began on the equator near the date line and turned northwestward at 160°E.

Disturbances in the central and western Pacific with 6–10-day periods have been studied by Nitta and Takayabu (1985), Lau and Lau (1990), and Chang et al. (1996). Because of the statistical techniques used, they were unable to define the wave type but were able to show a clear series of waves originating near the date line along the equator propagating west-northwestward into the western Pacific. These disturbances have a wavelength of 2500–3500 km and a westward phase speed of approximately 4–5 m s^{-1}. The disturbance track identified by Chang et al. (1996) is similar to that shown by Takayabu and Nitta (1993) for the 3–5-day disturbances discussed previously. Although they exhibit similar storm tracks, the relationship between the 3–6-day and 6–10-day disturbances is unclear. Liebmann and Hendon (1990) and Hendon and Liebmann (1991) showed that both ranges contained significant power in the 850-hPa meridional wind and OLR, respectively, between 135°E and 180°. Chang et al. (1996) showed that the 6–10-day disturbances can carry up to 28% of the total variance in the lower-tropospheric meridional wind.

The role of these westward-propagating disturbances in tropical cyclogenesis in the western Pacific remains uncertain. Briegel and Frank (1997) estimated that no more than 20% of tropical cyclones formed in association with TD-type disturbances. Ritchie (2000, personal communication; see also Ritchie and Holland 1999) suggested that nearly 50% of western Pacific tropical cyclones formed in association with TD-type disturbances. Most of these occurred near the eastern end of the monsoon trough, where westerlies meet easterlies. Sobel and Bretherton (1999) and Kuo et al. (2001) noted that an MRG wave propagating into such a region of zonal wind convergence could amplify and be reduced in scale via a wave accumulation process. Because MRG waves behave progressively more like Rossby waves as their scale decreases, the transition to TD-type disturbances could in principle relate to such background flow variations. This idea is consistent with the results of Liebmann and Hendon (1990, their Fig. 6), who showed that the transition zone occurred where the time-mean zonal wind was convergent.

Takayabu and Nitta (1993) presented a brief sequence of weather maps showing tropical cyclogenesis within a TD-type disturbance that apparently had transitioned from an MRG wave. Nitta and Takayabu (1985) and Chang et al. (1996) were able to track the origins of the 8–9-day disturbances that became tropical cyclones in the western Pacific back to a location near the equator and the date line, suggesting that those tropical cyclones might have had their origin in equatorial mode disturbances.

In addition to the synoptic-scale disturbances described above, the larger-scale Madden–Julian oscillation (MJO; see Madden and Julian 1994) is known to influence western Pacific tropical cyclogenesis (e.g., Gray 1979; Yamazaki and Murakami 1989; Liebmann et al. 1994). Liebmann et al. (1994) and Ferreira et al. (1996) have argued that tropical cyclogenesis is favored within the trailing lower-tropospheric equatorial Rossby gyres associated with the MJO convection. Alternatively, synoptic-scale disturbances may develop or intensify within the region of active MJO convection. This may occur by direct convective forcing of the disturbances or indirectly via disturbance growth in a region of negative meridional gradient of potential vorticity (Molinari et al. 1997; Ferreira and Schubert 1997; Dickinson and Molinari 2000). In support of these arguments, Nakazawa (1986) found that the amplitude of the 3–10-day variations of OLR was largest during the convectively active phase of the MJO. Similar evidence of disturbance growth was found by Yamazaki and Murakami (1989), Takayabu and Murakami (1991), Sui and Lau (1992), and Hendon and Liebmann (1994). Sobel and Maloney (2000) found a larger rate of wave accumulation occurs during the convectively active phase than the inactive phase of the MJO. These growing synoptic-scale waves during the active MJO could be the locus of subsequent tropical cyclogenesis.

Overall, previous work in the literature shows a storm track in the lower troposphere that originates near the equator in the central Pacific and ends well north of the equator in the western Pacific, where tropical cyclones tend to form. The disturbances that make up the storm track appear to be either 3–6-day or 6–10-day disturbances. Although various aspects of the problem have been studied in isolation, the interrelationship between the MJO, the apparent transition of equatorial to off-equatorial disturbances, and the genesis of tropical cyclones has not been fully examined. In the current study, the disturbances of interest are part of a large-amplitude packet of waves that fall within the 6–10-day period. The packet was discovered serendipitously in the equatorial meridional wind while examining cross-equatorial flow in the western Pacific. The large amplitude of these winds at the equator raised the possibility that equatorial modes were involved, particularly mixed Rossby–gravity waves. The intent of this work is to identify the nature of this packet and to describe its temporal and spatial evolution. In addition, three tropical cyclones formed in succession as the disturbances within the packet moved north of the equator. The evolution of the disturbances prior to tropical cyclone formation and the role of the MJO in the entire process will be examined.

2. Data and methodology

This study employs twice daily European Centre for Medium-Range Forecasts (ECMWF) uninitialized gridded analyses obtained from the National Center for Atmospheric Research (NCAR). The grids were obtained

on a 1.125° latitude–longitude grid on 12 pressure levels. All fields were interpolated to isentropic surfaces following Molinari et al. (1995).

Previous studies support the use of ECMWF analyses in the Tropics. ECMWF gridded analyses have been used to study both synoptic- and planetary-scale tropical waves (e.g., Reed et al. 1988; Liebmann and Hendon 1990; Lau and Lau 1990; Hendon and Liebmann 1991; Takayabu and Nitta 1993; Dunkerton 1993; Dunkerton and Baldwin 1995; Molinari et al. 2000; Molinari and Vollaro 2000). Although these studies focused on waves of different spatial and temporal scales, each showed that there was excellent agreement between the ECMWF gridded analyses and independently derived observational data, such as OLR. Dunkerton (1993) and Dunkerton and Baldwin (1995) found that wave properties determined from the ECMWF analysis were consistent with those determined from the radiosonde network in the western Pacific.

OLR will be used as a proxy for deep tropical convection. Wheeler and Kiladis (1999) recently showed that OLR fields could identify the MJO and convectively coupled wave signatures in the Tropics. A twice-daily OLR dataset was obtained from the NOAA–CIRES Climate Diagnostics Center on a 2.5° latitude–longitude grid. A description of the dataset is provided by Liebmann and Smith (1996).

Each field was filtered in time at each grid point using a Lanczos filter (Lanczos 1956; Duchon 1979). A low-pass filter with a 20-day cutoff period was used to isolate the background state (including the MJO scale). No detrending of the data was done; the low-pass filter thus includes seasonal variability. Two ranges of bandpass filtering were done to isolate synoptic-scale disturbances: 3–6-day and 6–10-day ranges. This study will focus on the latter, for reasons noted in section 3c.

3. Results

a. Wave structure along the equator

Figure 1a shows a longitude–time (Hovmöller) plot of the unfiltered meridional wind component (V) on the 315-K surface (near 700 hPa) and unfiltered OLR (shaded in regions of active convection) along the equator. Similar diagrams at nearby vertical levels and latitudes yielded nearly identical results and are not shown. The case study covers a period from June to early August 1987. A cluster of active deep convection, originating over the western Pacific (125°–135°E) during late June, propagates eastward and reaches 162°W by late July. This convective event is followed by a period of minimal deep convection that also propagates eastward. The convective/nonconvective sequence shown in the OLR field is suggestive of the MJO.

An examination of Fig. 1a shows that the unfiltered equatorial meridional wind has largest amplitude during the periods of active convection. The presence of sloping northerly to southerly flow couplets is suggestive of westward-propagating disturbances, but the fields are noisy.

Figure 1b shows the same fields as Fig. 1a after time filtering. Shown are the 6–10-day filtered meridional wind component ($\tilde{V}_{6-10}$) and low-pass-filtered OLR. As a result, Fig. 1b shows wave propagation in the contoured field and a measure of the MJO in the shaded field. The latter represents the background field through which the waves are passing. Figure 1b shows that the 6–10-day disturbances have a westward phase speed of approximately 3.5–4 m s^{-1} and wavelength of 2500–3000 km within the region of active background convection (these values will appear more clearly in subsequent figures). The westward phase speed increases to about 7 m s^{-1} in the western Pacific outside the active MJO. The development of a wave packet is evident in the $\tilde{V}_{6-10}$ contours. The zonal group speed is obtained from the axis that passes through the absolute maxima of $\tilde{V}_{6-10}$ in Fig. 1b, reflecting an eastward group speed of approximately 1 m s^{-1}. Both the phase and group speeds are substantially smaller than for the longer MRG waves described by Wheeler and Kiladis (1999).

Figures 2a–e show the values of $\tilde{V}_{6-10}$ as a function of longitude along the equator plotted every 2 days for the periods: 24–30 June (Fig. 2a), 2–8 July (Fig. 2b), 10–16 July (Fig. 2c), 18–24 July (Fig. 2d), and 26 July–1 August (Fig. 2e), respectively. The solid black curve at the bottom of each plot represents the background OLR along the equator, time averaged over each period. Shading indicates a period of active convection, identified by OLR values less than 220 W m^{-2}.

During the first period (Fig. 2a), the combination of $\tilde{V}_{6-10}$ curves outlines the initial amplification of the wave packet near 145°E. The packet is developing in the region of background convection associated with the beginning of the active MJO. The amplitude of the wave packet increases in association with the strengthening MJO convection (Fig. 2b).

During the 10–16 July period (Fig. 2c), both the MJO and wave packet reach their greatest magnitude. The difference in the MJO and wave packet speeds is evident during this period as the deepest convection has propagated eastward ahead of the wave packet. The change in the disturbance half wavelength, moving east to west across the packet, appears to be related to the change in the background convection. In the eastern portion of the packet where the background convection is active, the disturbance half wavelength is small compared to the western portion of the packet, where the background convection is inactive.

From 18–24 July (Fig. 2d), little active convection is observed in the western Pacific as the inactive phase of the MJO has begun. Finally, during the last period (Fig. 2e), active deep convection is absent throughout the domain. The combination of 6–10-day meridional wind curves reveals that the wave packet no longer has significant amplitude and can no longer be identified.

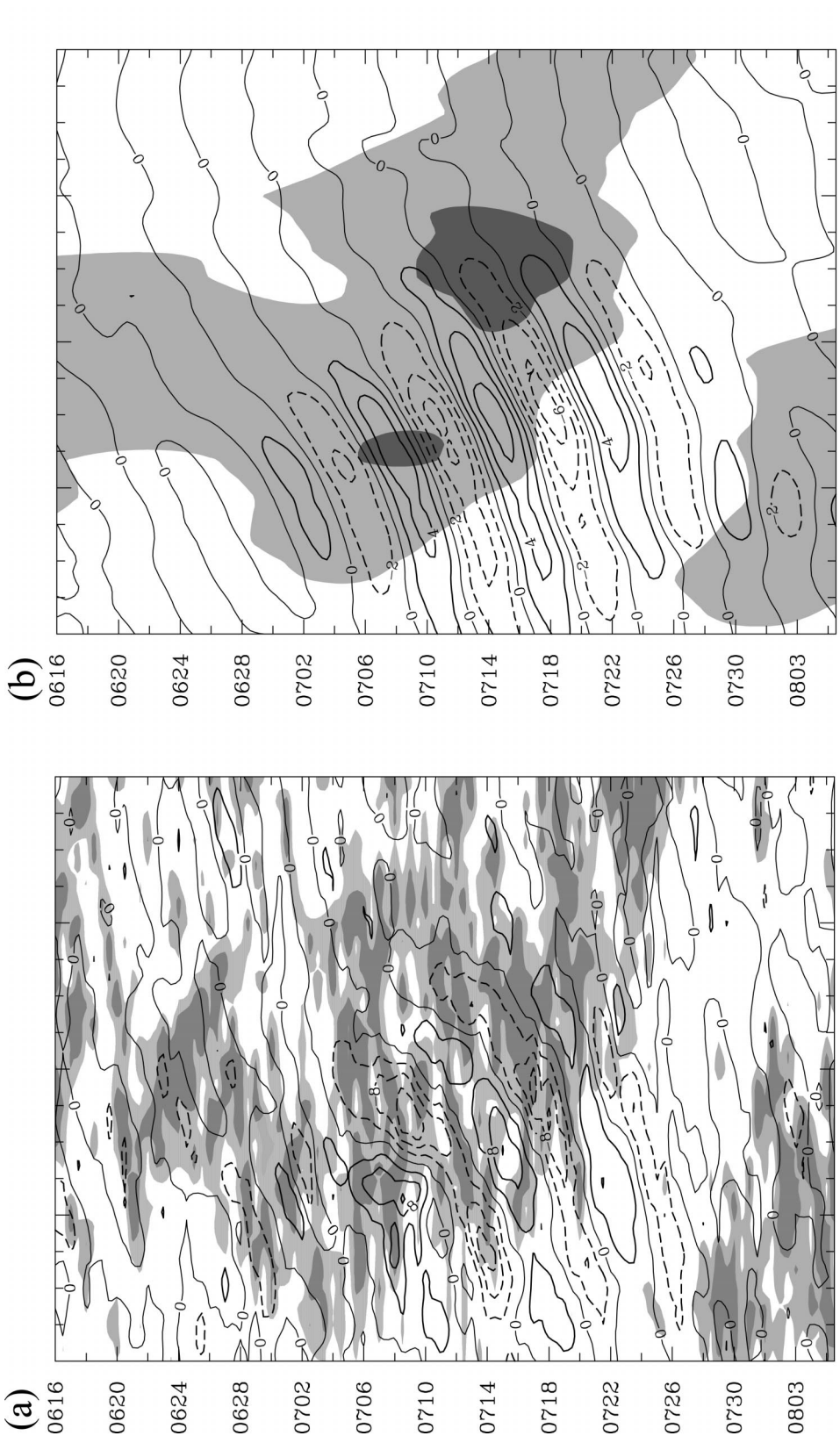

FIG. 1. Longitude–time plot of (a) the unfiltered meridional wind at the equator on the 315-K surface (contoured) and unfiltered OLR at the equator (shaded) and (b) 6–10-day bandpass-filtered meridional wind (contoured) and the low-pass-filtered (background) OLR at the equator (shaded). Contour interval of 2.5 m s^{-1} for the wind in (a) and 1.5 m s^{-1} in (b). Light shading represents OLR between 180 and 220 W m^{-2}; dark shading represents OLR below 180 W m^{-2} in both figures.

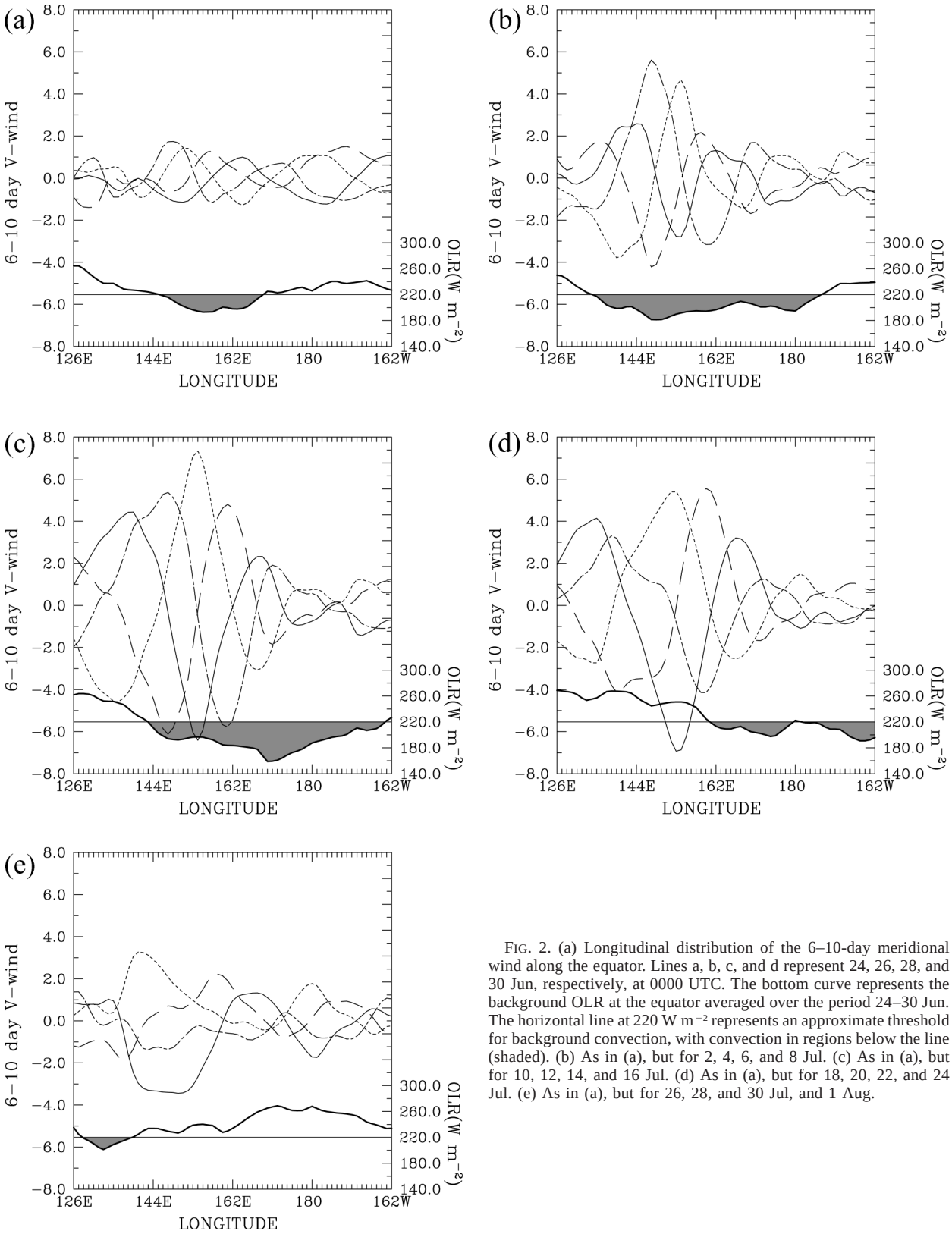

FIG. 2. (a) Longitudinal distribution of the 6–10-day meridional wind along the equator. Lines a, b, c, and d represent 24, 26, 28, and 30 Jun, respectively, at 0000 UTC. The bottom curve represents the background OLR at the equator averaged over the period 24–30 Jun. The horizontal line at 220 W m^{-2} represents an approximate threshold for background convection, with convection in regions below the line (shaded). (b) As in (a), but for 2, 4, 6, and 8 Jul. (c) As in (a), but for 10, 12, 14, and 16 Jul. (d) As in (a), but for 18, 20, 22, and 24 Jul. (e) As in (a), but for 26, 28, and 30 Jul, and 1 Aug.

TABLE 1. Group and phase speeds from the MRG plane wave equation.

Equivalent depth (m)	λ = 2500 km		λ = 3000 km	
	Cp (m s^{-1})	Cg (m s^{-1})	Cp (m s^{-1})	Cg (m s^{-1}
1	−2.2	0.9	−2.8	1.0
10	−2.8	1.8	−3.8	2.1
25	−3.1	2.2	−4.1	2.7
50	−3.2	2.5	−4.4	3.1
100	−3.3	2.7	−4.6	3.5
Observed	Cp = −3.8		Cg =1	

Disturbance wavelengths can be estimated accurately from Fig. 2 by measuring the peak-to-peak or trough-to-trough distances. Within the region of active convection, the disturbance wavelength increases from approximately 2300 km in Fig. 2a to approximately 3000 km in Fig. 2d. This increase might relate to dispersion of the waves within the packet. By tracking the spacing between the peaks (or troughs), it appears that the wavelength and phase speed increase outside the convective region.

The series of equatorial $\tilde{V}_{6\text{–}10}$ curves in Fig. 2 illustrates the process of wave packet growth in the western Pacific during this event. An eastward moving wave packet, containing westward propagating disturbances, develops within a convectively active MJO, resulting in an amplitude increase in the wave packet and, hence, amplification of the individual disturbances within the packet.

The westward propagating disturbances in Figs. 1b and 2 have a large $\tilde{V}_{6\text{–}10}$ at the equator. Since $n = 1$ equatorial Rossby waves have no meridional component at the equator (e.g., Kiladis and Wheeler 1995), the disturbances shown in Fig. 1b are not equatorial Rossby waves. Rather, the large equatorial meridional wind component suggests that the disturbances are MRG waves. The plane wave equation for an MRG wave, given by Gill [1982; his Eq. (11.6.9)], can be written as $\omega^2 - kc\omega - \beta c = 0$, where k is the horizontal wavenumber, ω is the frequency, β is the planetary vorticity gradient, and c is the shallow-water gravity wave speed ($\sqrt{gH}$, where H is the equivalent depth). Solving the plane wave equation for ω and keeping the negative root, the phase and group speeds are given by $1/2[c - 1/k(c^2k^2 + 4\beta c)^{1/2}]$ and $1/2c[1 - ck(c^2k^2 + 4\beta c)^{-1/2}]$, respectively. Because the background zonal flow across the wave packet varies from weak westerly to weak easterly, the zonal wind was assumed to be zero in the above calculation. Table 1 shows the phase and group speeds obtained when the observed wavelengths are inserted into the plane wave equation, for a variety of equivalent depths. Because the observed waves have large amplitude and are convectively active, an exact match between the observed and theoretical group and phase speeds is not expected. Differences between the theoretical and observed group speeds will also occur because the calculated values represent disturbances of one wavelength and not a group of waves within a packet. The combined differences between the observed (Fig. 1b) and calculated phase and group speeds are minimized for equivalent depths from 10 to 25 m, consistent with the results of Wheeler and Kiladis (1999).

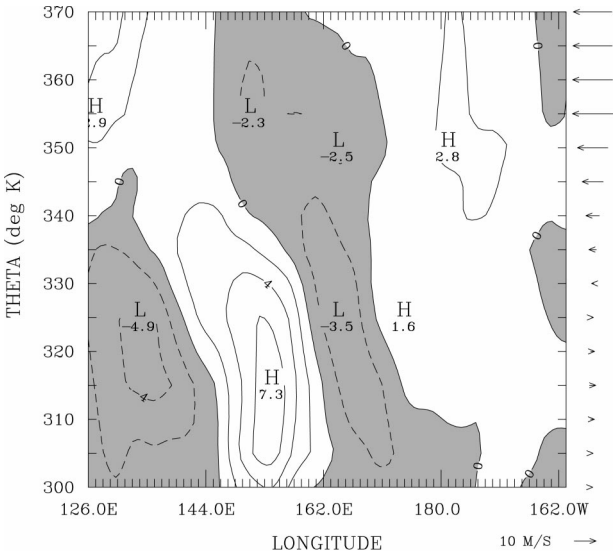

FIG. 3. Vertical cross section of the 6–10-day meridional wind along the equator on 0000 UTC 14 Jul. Contour interval of 1.0 m s^{-1}. Wind vectors on the right show the vertical profile of the longitudinally averaged (from 126°E to 180°) background zonal wind.

The vertical cross section along the equator of $\tilde{V}_{6\text{–}10}$ on 14 July, close to the time of largest wave amplitude, is shown in Fig. 3. The arrows on the far right of Fig. 3 represent the longitudinally averaged (from 126°E to 180°) unfiltered zonal wind component along the equator. Average pressure on the isentropic surfaces ranges from 967 hPa at 300 K to 119 hPa at 370 K. Westerly flow is confined to the lowest levels (325 K and lower), reflecting the influence of the MJO on the zonal wind. Small vertical wind shear is present below 325 K (about 550 hPa). Above 325 K, the flow becomes easterly and increases with height.

Figure 3 shows that the 6–10-day disturbances have largest amplitude below 330 K. Near the date line the disturbances tilt westward. The disturbance tilt changes in the western Pacific. The disturbances are nearly vertical in the lower troposphere. Above 335 K (460 hPa), the downshear tilt of the disturbances is more pronounced. This structure suggests that the source of the wave energy is in the lower troposphere, and that energy propagates upward and is lost to the mean flow above the lower troposphere.

The mean vertical wind shear on the equator in Fig. 3 resembles that of RR71 at the island of Koror (7°N, 135°E): weak low-level westerlies, easterly shear, and strongest easterlies in the upper troposphere. The vertical structure of RR71's TD-type disturbances in the vicinity of Koror (their Fig. 10a) resembles that in Fig. 3, especially the reversal of meridional wind from lower

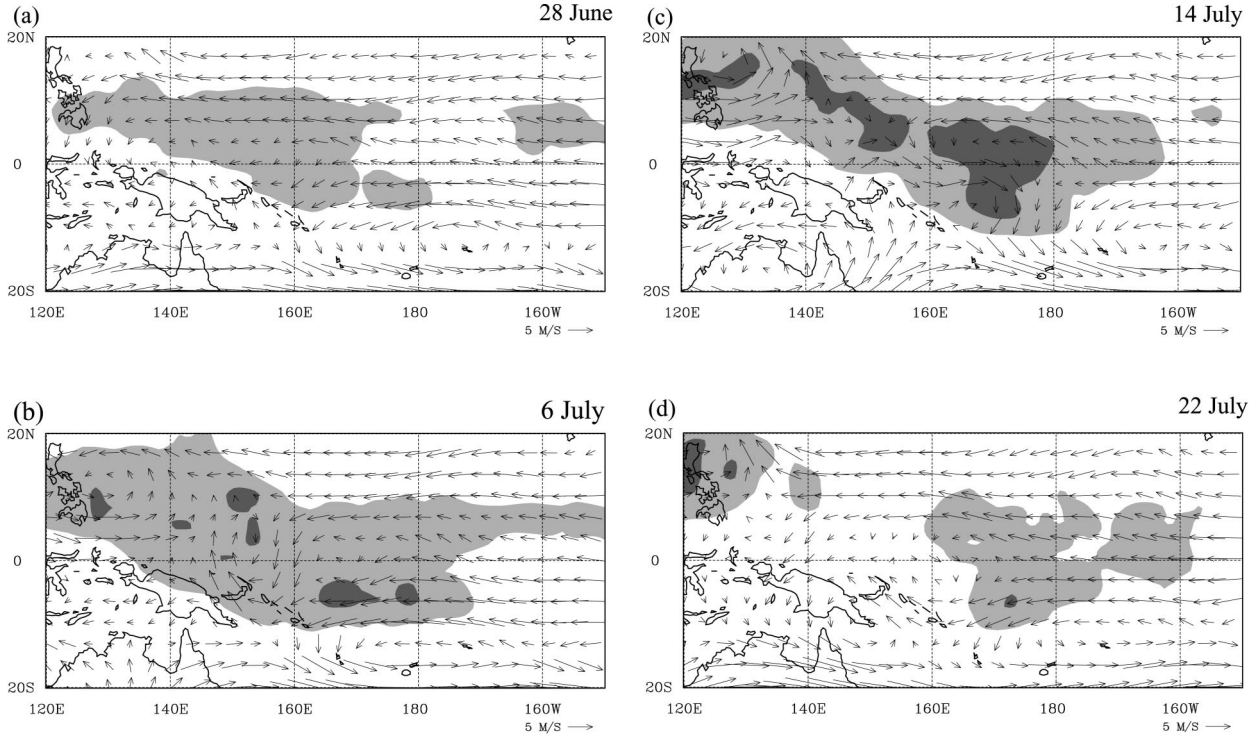

FIG. 4. Background (low-pass-filtered) OLR (light shading for values between 180 and 220 W m^{-2}; dark shading for values below 180 W m^{-2}) and background wind vectors at 0000 UTC on (a) 28 Jun, (b) 6 Jul, (c) 14 Jul, and (d) 22 Jul. The vector spacing is 3.375°, representing every third point from the ECMWF analyses.

to upper troposphere and the downshear tilt with height. At other longitudes east of 135°E, however, RR71's vertical wind shear and vertical structure differ from that shown here. In addition, RR71's disturbances had periods of about 5 days. It appears unlikely they represent the same type of disturbance as those shown here.

b. Background flow evolution

Figure 4 shows *x–y* plots of the evolution of the low-pass-filtered wind and OLR. As noted earlier, the term ''background'' will be used to identify the low-pass-filtered fields, which can be viewed as the slowly varying flow through which the 6–10-day disturbances propagate. Consistent with Fig. 1, only regions likely to contain active convection in the background (OLR <220 W m^{-2}) are shaded. Figure 1b shows that the wave packet was best-defined between late June and late July, and the four panels of Fig. 4 are evenly distributed over this period.

On 28 June (Fig. 4a), the active MJO had overspread the region. Background convection was strongest in the Northern Hemisphere, but extended south of the equator from about 150°–170°E. Virtually no westerly flow existed along the equator at this time. The zonal wind was broadly convergent west of about 170°E. This suggests that wave accumulation may, in part, be responsible for the development of the wave packet (Figs. 1b, 2a).

By 6 July (Fig. 4b), the MJO expanded eastward and amplified. Convection was active on both sides of the equator from 140°E to the date line. Westerly flow existed on the equator at the western end of the region, and easterly flow at the eastern end of the active MJO envelope. Zonal wind convergence was confined to small regions. This suggests that wave accumulation was not responsible for the observed strengthening of the wave packet during this period (Figs. 1b, 2b). A well-defined cyclonic circulation accompanied the strong convection within the active MJO well north of the equator near 130°E. Cyclonic Rossby gyres grew in each hemisphere between 160°E and 180°. During this period the wave packet (Fig. 1b) was in a rapid growth phase.

A large clockwise gyre centered near the equator developed by 6 July at about 152°E. The cause of this gyre, which does not represent any aspect of Gill's (1980) solutions for symmetric or asymmetric heating, is not certain. It is notable that this feature was at its maximum amplitude when easterlies crossed the mountainous island of New Guinea (Fig. 4b), whereas it decayed when easterlies over the island ceased (Fig. 4c).

By 14 July (Fig. 4c), both the active MJO and the wave packet had achieved maximum amplitude. Westerly flow on the equator extended from the west end of the region near 120°E all the way to about 175°E. At this time the heating was somewhat symmetric about

the equator east of 160°E, and strongly asymmetric west of 160°E. The cyclonic gyre to the northwest had strengthened and moved north of 15°N. The cyclonic equatorial Rossby gyres had strengthened as well.

By 22 July (Fig. 4d), the active MJO had moved eastward and decayed, and once again no westerlies were present along the equator. All of the gyres described above had considerably weakened.

Overall, the evolution of the low-pass-filtered flow during the passage of the active MJO was fairly typical, with the exception of the large clockwise gyre upstream from New Guinea. From the point of view of this case study, the most significant aspects of the low-pass evolution were (i) the equatorial Rossby gyres characteristic of Gill's (1980) solution were present only east of 160°E, where heating most persistently straddled the equator; (ii) west of 160°E, heating remained strongest north of the equator; and (iii) the active MJO pattern extended northwestward west of about 150°E, with strongest heating mostly poleward of 10°N at the western end of the region.

c. Wave transition and tropical cyclogenesis

It was argued earlier that the 6–10-day disturbances have the characteristics of MRG waves at the equator. As noted in the introduction, however, MRG waves in the Pacific have been found predominantly on a 3–6-day timescale. Disturbances in the 6–10-day range have been described (Lau and Lau 1990; Chang et al. 1996), but no wave type has been identified in these disturbances.

Figure 5 shows the variance of both the 3–6-day and 6–10-day meridional wind component, averaged from 30 June to 30 July, which encompasses the presence of the wave packet. Also shown (shaded) is the region in which the mean OLR over the period was below 220 W m^{-2}, indicative of active mean convection. Variance of the 3–6-day meridional wind was largest away from the equator, particularly downstream of the initial appearance of three tropical depressions that formed during the period (the latter shown by hurricane symbols). A tropical cyclone moving at 5 m s^{-1} with a perturbation wind 1500–2000 km wide would fall firmly within the 3–6-day filter. The maximum 3–6-day variance along the equator was small, about 5 m^2 s^{-2}.

Figure 5b shows the variance of the 6–10-day meridional wind. East of about 150°E, variance was largest at or near the equator. Maximum equatorial variance exceeded that of the 3–6-day disturbances by a factor of 3. West of 145°E, maximum variance clearly shifted north of the equator. This suggests that the apparent MRG waves identified earlier were undergoing some sort of a transition west of 150°E. The maximum 6–10-day variance occurred in a region of asymmetric mean heating about the equator.

The 6–10-day disturbances represented more than 30% of the total variance (not shown) along the equator

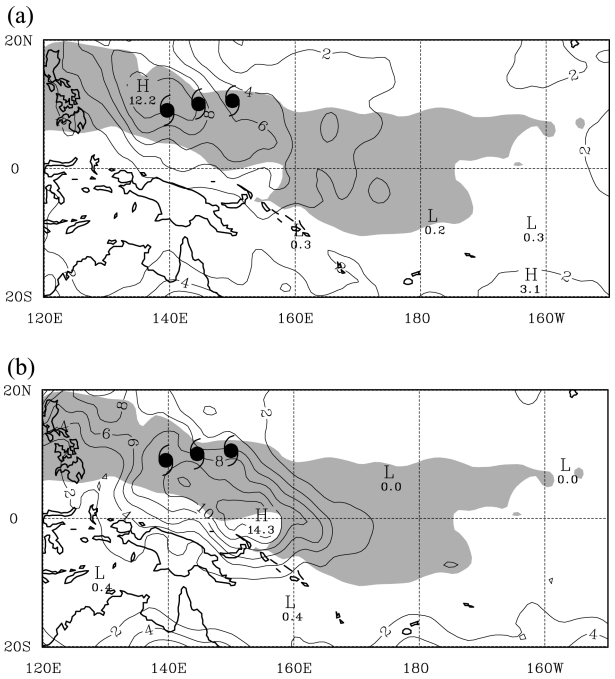

FIG. 5. Time-mean (30 Jun–30 Jul) OLR (shaded values <220 W m^{-2}) and (a) 3–6-day and (b) 6–10-day meridional wind variance. Contour interval for variances 2 m^2 s^{-2}. The tropical cyclone symbols mark the positions of tropical depression formation, as defined by the Joint Typhoon Warning Center.

from 170° to 120°E, and as much as 65% of total variance just south of the equator at 150°E. The 6–10-day percent variance fell below 30% everywhere poleward of 15°N. In contrast, the 3–6-day meridional wind carried less than 30% of the total variance along the equator at all longitudes, and had maximum variance poleward of 10°N. It is argued that combining the two periods (as done, for instance, by Nakazawa 1986) would be unwise because it might mix two wave types. While previous work (Dunkerton and Baldwin 1995; Wheeler and Kiladis 1999) leaves no doubt that MRG waves show most clearly in the 3–6-day range, it appears that during the occurrence of this large-amplitude wave packet, such waves are not the primary feature. For the remainder of this paper the focus will be on the 6–10-day disturbances.

In order to investigate the track of the disturbances during the transition and their relationship to the MJO, Fig. 6 shows a sequence of synoptic maps from 0000 UTC 28 June 1987 to 0000 UTC 24 July 1987 every 2 days using 6–10-day bandpass-filtered winds and background OLR. Because all circulations in the bandpass-filtered winds end up in the Northern Hemisphere, clockwise circulations will be labeled ''anticyclonic'' and counterclockwise circulations will be labeled ''cyclonic.'' Following Magaña and Yanai (1995), the disturbances will be given unique labels to allow them to be followed over several days.

A weak cyclonic disturbance (labeled ''A'') appears

in the wind field on 28 June (Fig. 6a) just north of the equator at about 150°E, within the active MJO convection. By 30 June a train of weak disturbances is centered just north of the equator within the expanding MJO signal. Disturbance A has moved westward, and is followed by strong anticyclonic disturbance B and hints of a cyclonic disturbance further east. During the next 4 days (Figs. 6c,d), disturbance A becomes hard to track, but disturbance B continues westward and amplifies as it crosses 150° and 140°E. A strong negative $\tilde{V}_{6-10}$ component along 150°E extends from near 20°N to 7°S. Cyclonic disturbance C appears at this time and grows in amplitude between then and 8 July (Figs. 6e,f). At the latter time, the $\tilde{V}_{6-10}$ component along 150°E has reversed sign and become strongly positive. A tropical depression (eventually Tropical Storm Thelma, labeled 1) forms at the northern extent of this southerly flow at 13.9°N, 148.9°E on 0000 UTC 8 July. The depression forms in a region where $\partial v/\partial x$ is positive and where convection would be expected with an MRG wave, not at the center of disturbance C, which has moved northwestward to about 5°N by this time. At the same time, disturbance B has moved northwestward to 10°N (Fig. 6e), and both B and C have developed a southwest–northeast tilt. A similar tilt was found in the same region by Liebmann and Hendon (1990), Lau and Lau (1990), and Chang et al. (1996). Clockwise disturbance D and counterclockwise disturbance E are also visible in the wind field on 8 July (Fig. 6f) further to the east as both the MJO and the wave packet grow in areal coverage. Disturbance E is nearly directly on the equator at about 170°E.

Figures 6g–n show two additional cycles of the above sequence of MRG wave evolution and tropical cyclone formation. The wave packet continues to grow in amplitude on 10–12 July (Figs. 6g,h). Disturbances C and D move northwestward toward 20°N. Cyclonic disturbance E moves west-northwestward and amplifies (Figs. 6i,j), similarly to disturbance C earlier. A tropical depression (eventually Tropical Storm Vernon, labeled 2) develops in the same part of the disturbance, at the edge of the northerlies and where $\partial v/\partial x$ is positive, at 11.3°N and 142.0°E on 0000 UTC 16 July (Fig. 6j). A third cycle is shown in Figs. 6k–n, with disturbances first appearing near 170°E on or just south of the equator, then moving westward and slightly northward to 150°E while amplifying, then maintaining amplitude as they move northwestward between 145° and 120°E. The final tropical cyclone in the sequence (eventually Tropical Storm Alex, labeled 3) occurs with the third cyclonic disturbance (G; Fig. 6m) at 9.3°N, 139.5°E on 0000 UTC 22 July. The latter does not develop at the northern extent of the equatorial northerlies, but north of the center of the cyclonic disturbance. Formation still occurs in the vicinity of positive $\partial v/\partial x$. By 24 July (Fig. 6n), the MJO has nearly disappeared, and no amplification of disturbances or tropical cyclone formations occur thereafter.

Figure 6 shows that tropical cyclone formation occurred in association with three consecutive cyclonic circulations within the wave packet. The tropical cyclones did not form in the region of trailing Rossby gyres centered near 170°E (see Figs. 4b–d), as proposed by Liebmann et al. (1994) and Ferreira et al. (1996). Rather, formation occurred between 139° and 150°E, and 5° and 15°N, in a region where the background convection was persistently asymmetric with respect to the equator.

Figure 6 showed the off-equatorial turning of 6–10-day disturbances and their relationship to the background heating field. There seems to be little doubt that some sort of transition must have occurred west of 150°E. In order to examine this process in more detail, Fig. 7 shows the 6–10-day structure of both winds and OLR during the period the wave packet was reaching its largest amplitude. Of interest is the change in the structure of convection within the disturbances as they moved westward. Figure 7a, valid at 0000 UTC 10 July just after the formation of the first tropical depression, shows a clear TD-type structure in cyclonic disturbance C (lettering is identical to that in Fig. 6), which was filled with cloud. Anticyclonic disturbance D had no active convection at its center. It contained a Southern Hemisphere convective maximum in the vicinity of equatorial northerlies, and a Northern Hemisphere maximum at the tail of equatorial southerlies. These maxima were not at the same latitudes, and thus did not represent a clear MRG wave signature. Rather, they seem to indicate an MRG-like signature that had shifted northward away from the equator. Cyclonic disturbance E, on the equator further east, had a complex convective signature. Because it was clear in the center, it did not have a TD-type structure.

Two days later on 12 July (Fig. 7b), disturbance D remained clear at the center, as would be expected in a TD-type disturbance. Disturbance E appeared to have both MRG and TD-type structure: convective maxima at the leading edge of the equatorial northerlies and southerlies, but also convection beginning to fill the center. Disturbance F on the equator further east had no clear signature.

By 14 July (Fig. 7c), cyclonic disturbance E became filled with cloud at its center as it moved west-northwestward to about 5°N. Cloudiness also extended northeastward ahead of cross-equatorial southerlies. A tropical depression formed in association with disturbance E between 14 and 16 July (Fig. 7d). It is notable that it formed not in the center of E, but rather in the extension of clouds to the northeast that appeared to represent the memory of the MRG history of the disturbance. Anticyclonic disturbance F showed a fairly clear MRG signature at this time.

Figure 7 shows that disturbances on the 315-K level continued to strengthen as they turned away from the

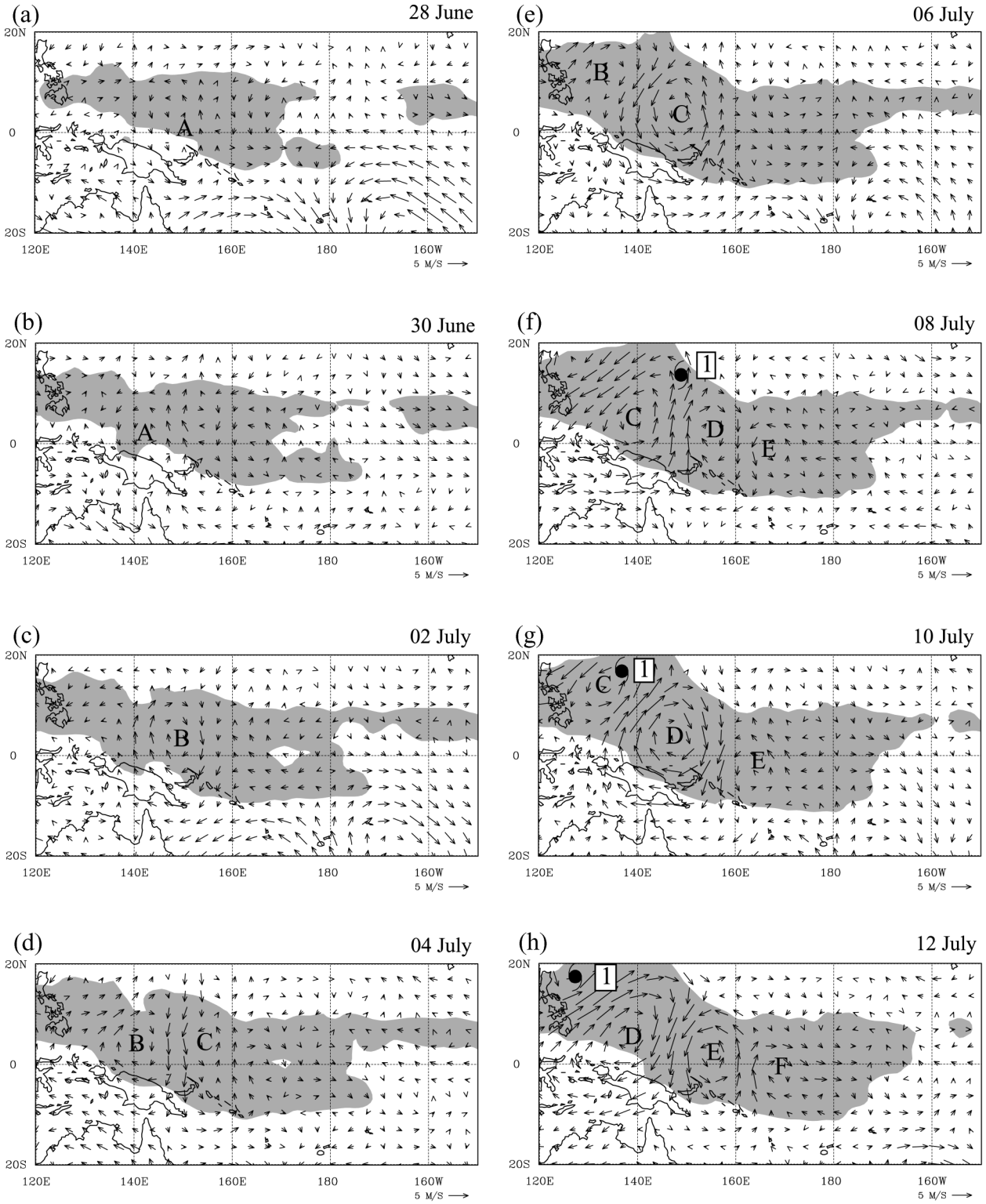

FIG. 6. 6–10-day vector winds on the 315-K surface plotted with background OLR (shaded <220 W m^{-2}) at 0000 UTC on (a) 28 Jun, (b) 30 Jun, (c) 2 Jul, (d) 4 Jul, (e) 6 Jul, (f) 8 Jul, (g) 10 Jul, (h) 12 Jul, (i) 14 Jul, (j) 16 Jul, (k) 18 Jul, (l) 20 Jul, (m) 22 Jul, and (n) 24 Jul. The vector spacing is 3.375°, representing every third point from the ECMWF analyses. Numbered hurricane symbols are shown from the depression stage onward, as defined by the Joint Typhoon Warning Center. The numbers 1, 2, and 3 refer to Tropical Storms Thelma, Vernon, and Alex, respectively.

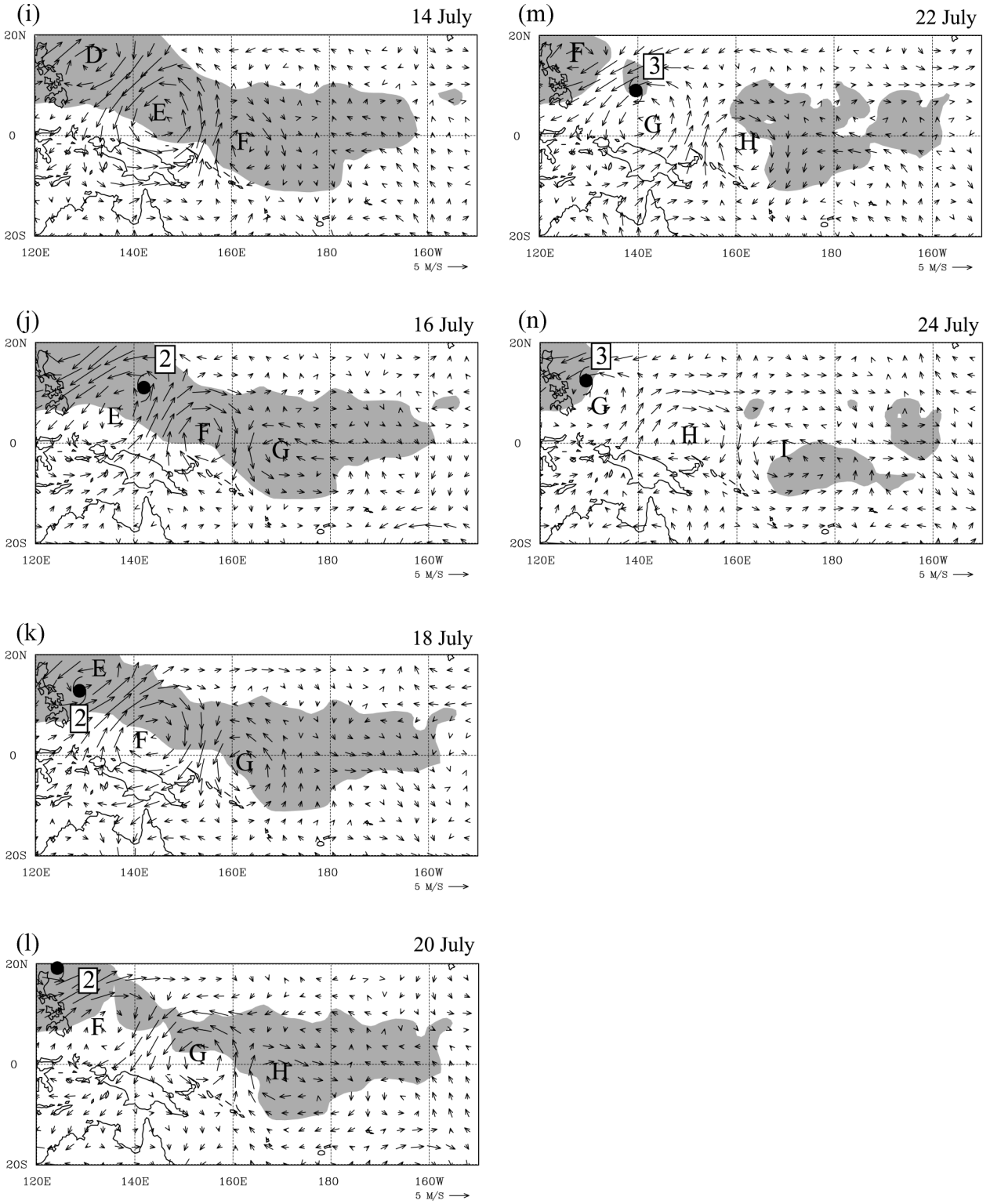

FIG. 6. (*Continued*)

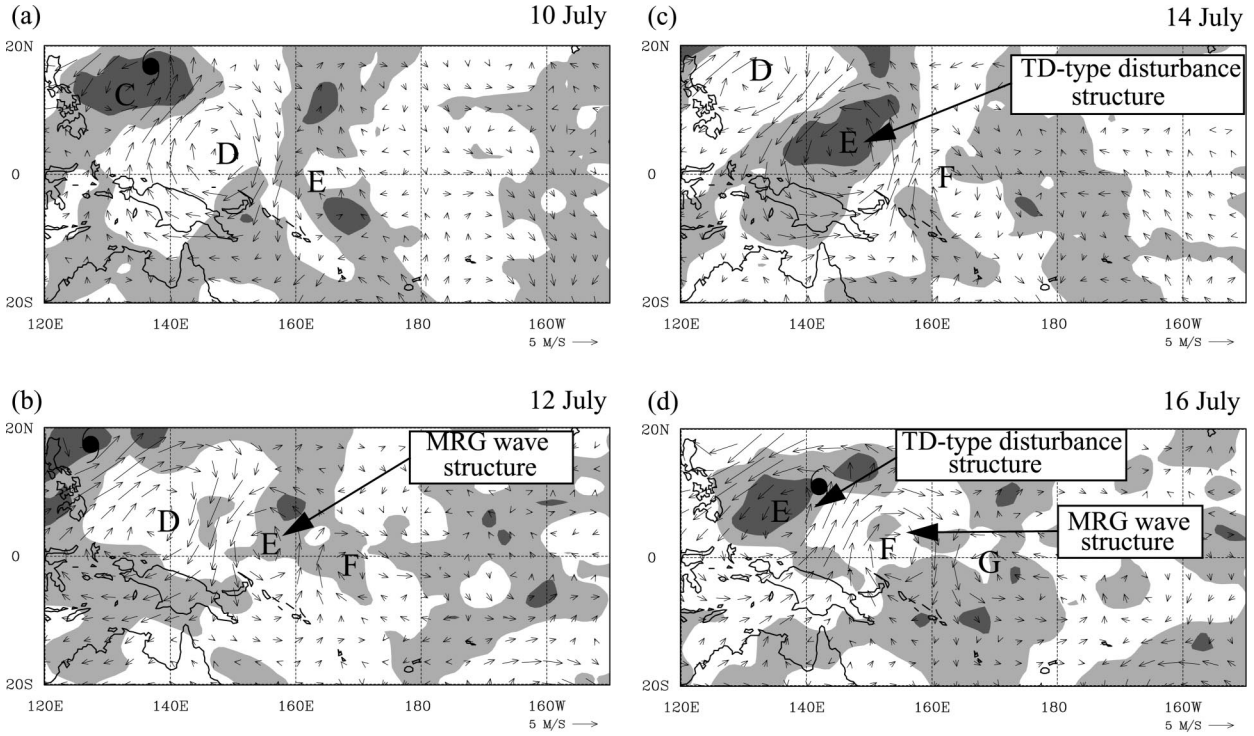

FIG. 7. 6–10-day wind vectors on the 315-K surface plotted with 6–10-day OLR (light shading for values between 0 and -20 W m^{-2}; dark shading for values below -20 W m^{-2}) at 0000 UTC (a) 10 Jul, (b) 12 Jul, (c) 14 Jul, and (b) 16 Jul. The vector spacing is 3.375°, representing every third point from the ECMWF analyses. The labelling of disturbances and tropical cyclones is identical to those in Fig. 6.

equator. As this strengthening occurred, it became increasingly likely that a surface circulation would develop, according to potential vorticity attribution arguments (e.g., Thorpe 1985). Because the disturbances were no longer on the equator, Ekman pumping could then have been responsible for wave-scale convection in the cyclonic disturbances, and clearing in the anticyclones, as was observed.

In addition to this TD-type convective structure, some echo of MRG-like convection remained, and tropical depressions 1 and 2 formed in this extended convective region rather than in the center of the cyclonic disturbance. Tropical depression 3 also did not form in the center of the associated cyclonic disturbance, but north of it. The evidence suggests that tropical cyclogenesis occurred in the cyclonic part of disturbances that were making the transition from MRG to TD-type.

4. Discussion

One goal of this paper was to provide a synoptic study of a lower-tropospheric MRG wave packet in the western Pacific. It was felt that such a case study was the best means of describing the temporal and spatial evolution that ultimately led to repeated development of tropical cyclones. Although detailed weather maps have been shown, a number of dynamical issues remain unresolved. These include the following.

1) The MRG wave packet appeared and amplified within the convectively active envelope of the MJO, but the exact process by which this occurred is uncertain. The packet initially developed in a region of background flow convergence along the equator associated with the MJO (Figs. 4a,b), suggesting that wave accumulation played a role (Sobel and Bretherton 1999; Kuo et al. 2001). But it continued to amplify even after the equatorial background convergence moved well to the east (Figs. 4c,d). The packet existed in the presence of persistently asymmetric background convection about the equator, but the means by which such convection could produce amplification of a packet of 6–10-day period waves remains unclear.
2) The reason for the turning of the MRG waves out of the equatorial wave guide has not been addressed. The background flow (Fig. 4) and the total (unfiltered) wind (not shown) are generally not oriented to produce such a track. The asymmetric background heating may have altered the background zonal wind in such a way as to produce refraction of the waves away from the equator (M. Reeder 2000, personal communication). This mechanism might account for the initial deviation, but does not seem sufficient to account for the continued motion of disturbances poleward of 20°N. The disturbance track directly paralleled the envelope of active convection within

the MJO. As a result, any theory of wave behavior must account for the role of the MJO as well as the dynamics of the transition from an equatorial mode to a TD-type disturbance.

3) The relationship between the MRG waves in this study and the much longer MRG waves known to exist in the central Pacific is uncertain. The waves in this study had an initial wavelength of only 2300 km, 3–4 times smaller than those described by Dunkerton and Baldwin (1995). Dunkerton and Baldwin (1995) reported no tropical cyclogenesis within their waves, presumably because their scale was much too large. Yet they showed a similar transition to that shown here, both in the off-equatorial turning and the change in convective structure of the waves. In principle, wave accumulation could account for the reduction in scale from the central Pacific to the shorter waves found in this study. It is more likely that the MRG waves described here developed locally within the active MJO and were independent of those in the central Pacific. The disturbances in this study appear to relate most closely in period and wavelength to those found by Lau and Lau (1990) and Chang et al. (1996).
4) The actual process by which tropical cyclogenesis occurred within the transitioning waves could not be addressed in this study. It was hypothesized that Ekman pumping developed within the surface reflection of the disturbances once they had moved sufficiently far from the equator. Raymond et al. (1998), however, have argued that Ekman pumping plays no significant role in the early stages of tropical cyclogenesis. In addition, although the cyclonic disturbances filled with cloud as they moved away from the equator, the tropical cyclones developed on the edge of these disturbances, where convection is favored in the idealized MRG wave, not in the center. The details of the tropical cyclogenesis remain a topic for further research.

Despite the uncertainties described above, it is possible to describe a clear sequence of events that incorporates the MJO, the waves, and tropical cyclogenesis. The MRG wave packet first appeared coincident with the arrival of the MJO, and on a similar scale. The packet (and the individual waves within it) amplified as long as it remained within the active MJO, and quickly dispersed when the MJO moved eastward and left it behind. Individual MRG waves slowly increased in scale from 2300 to 3000 km, presumably due to slow dispersion in the presence of a convectively active background, then abruptly increased in scale and in propagation speed when the MJO left the region.

Consistent with MRG wave dynamics, the packet moved slowly eastward and the gyres within it moved westward. Both clockwise and counterclockwise gyres amplified as they moved along the equator, then northwestward, following the envelope of active convection within the MJO. As they moved away from the equator, the gyres retained aspects of the convective structure of MRG waves, even as the cyclonic gyres filled with cloud and the anticyclonic gyres lost their cloudiness. At this stage the disturbances seemed to have characteristics of both TD-type and MRG waves.

Tropical cyclogenesis did not occur within the trailing Rossby gyres associated with equatorially symmetric heating (Ferreira et al. 1996). Such Rossby gyres existed in this study but remained well east of the region of tropical cyclogenesis. Instead, tropical cyclogenesis occurred in association with each large-amplitude cyclonic circulation in the MRG wave packet, on the edge of the circulation where $\partial v/\partial x$ was largest and positive, consistent with the findings of Chang et al. (1996).

Although this study covered only one 5-week period, the correspondence of the disturbance tracks shown in Fig. 6 with those shown in bandpass-filtered 850-hPa meridional wind variance by Takayabu and Nitta (1993), and with the storm tracks shown by Nitta and Takayabu (1985), Lau and Lau (1990), and Chang et al. (1996), suggests that the events shown in this paper are not isolated occurrences. Future work will focus on how commonly MRG waves act as precursors to western Pacific tropical cyclogenesis, and on the dynamics of the MRG wave packet.

Acknowledgments. This work benefited greatly from discussions with Dr. Lloyd Shapiro of the University of Munich, Dr. Michael Reeder of Monash University, and Dr. Adam Sobel of Columbia University. The authors would like to thank the three anonymous reviewers and editor Dr. George Kiladis for their insightful comments. The authors would also like to thank David Vollaro and Anantha Aiyyer of the University at Albany for their comments. This research was supported by Office of Naval Research Grant N000149810599 and National Science Foundation through Grant ATM9900671.

REFERENCES

Briegel, L. M., and W. M. Frank, 1997: Large-scale influences on tropical cyclogenesis in the western North Pacific. *Mon. Wea. Rev.*, **125,** 1397–1413.

Chang, C.-P., J. M. Chen, P. A. Harr, and L. E. Carr, 1996: Northwestward-propagating wave patterns over the tropical western North Pacific during summer. *Mon. Wea. Rev.*, **124,** 2245–2266.

Dickinson, M. J., and J. Molinari, 2000: Climatology of sign reversals of the meridional potential vorticity gradient over Africa and Australia. *Mon. Wea. Rev.*, **128,** 3890–3900.

Duchon, C. E., 1979: Lanczos filtering in one and two dimensions. *J. Appl. Meteor.*, **18,** 1016–1022.

Dunkerton, T. J., 1993: Observation of 3–6-day meridional wind oscillations over the tropical Pacific, 1973–1992: Vertical structure and interannual variability. *J. Atmos. Sci.*, **50,** 3292–3307.

——, and M. P. Baldwin, 1995: Observation of 3–6-day meridional wind oscillations over the tropical Pacific, 1973–1992: Horizontal structure and propagation. *J. Atmos. Sci.*, **52,** 1585–1601.

Ferreira, R. N., and W. H. Schubert, 1997: Barotropic aspects of ITCZ breakdown. *J. Atmos. Sci.*, **54,** 261–285.

——, ——, and J. J. Hack, 1996: Dynamical aspects of twin tropical

cyclones associated with the Madden–Julian oscillation. *J. Atmos. Sci.,* **53,** 929–945.
Gill, A. E., 1980: Some simple solutions for heat-induced tropical circulation. *Quart. J. Roy. Meteor. Soc.,* **106,** 447–462.
——, 1982: *Atmosphere–Ocean Dynamics.* Academic Press, 662 pp.
Gray, W., 1979: Hurricanes: Their formation, structure, and likely role in the tropical circulation. *Meteorology over the Tropical Oceans,* D. B. Shaw, Ed., Royal Meteorological Society, 155–218.
Hendon, H. H., 1986: Streamfunction and velocity potential representation of equatorially trapped waves. *J. Atmos. Sci.,* **43,** 3038–3042.
——, and B. Liebmann, 1991: The structure and annual variation of antisymmetric fluctuation of tropical convection and their association with Rossby–gravity waves. *J. Atmos. Sci.,* **48,** 2127–2140.
——, and ——, 1994: Organization of convection within the Madden–Julian Oscillation. *J. Geophys. Res.,* **99,** 8073–8083.
Kiladis, G. N., and M. Wheeler, 1995: Horizontal and vertical structure of observed tropospheric equatorial Rossby waves. *J. Geophys. Res.,* **100,** 22 981–22 997.
Kuo, H.-C., J.-H. Chen, R. T. Williams, and C.-P. Chang, 2001: Rossby waves in zonally opposing mean flow: Behavior in northwest Pacific summer monsoon. *J. Atmos. Sci.,* **58,** 1035–1050.
Lanczos, C., 1956: *Applied Analysis.* Prentice Hall, 539 pp.
Lau, K.-H., and N.-C. Lau, 1990: Observed structure and propagation characteristics of tropical summertime disturbances. *Mon. Wea. Rev.,* **118,** 1888–1913.
Liebmann, B., and H. H. Hendon, 1990: Synoptic-scale disturbances near the equator. *J. Atmos. Sci.,* **47,** 1463–1479.
——, and C. Smith, 1996: Description of a complete (interpolated) outgoing longwave radiation dataset. *Bull. Amer. Meteor. Soc.,* **77,** 1275–1276.
——, H. H. Hendon, and J. D. Glick, 1994: The relationship between tropical cyclones of the western Pacific and Indian Oceans and the Madden–Julian Oscillation. *J. Meteor. Soc. Japan,* **72,** 401–411.
Madden, R. A., and P. R. Julian, 1994: Observations of the 40–50-day oscillation—A review. *Mon. Wea. Rev.,* **122,** 814–837.
Magaña, V., and M. Yanai, 1995: Mixed Rossby–gravity waves triggered by lateral forcing. *J. Atmos. Sci.,* **52,** 1473–1486.
Molinari, J., and D. Vollaro, 2000: Planetary- and synoptic-scale influences on eastern Pacific tropical cyclogenesis. *Mon. Wea. Rev.,* **128,** 3296–3307.
——, S. Skubis, and D. Vollaro, 1995: External influences on hurricane intensity. Part III: Potential vorticity evolution. *J. Atmos. Sci.,* **52,** 3593–3606.
——, D. Knight, M. Dickinson, D. Vollaro, and S. Skubis, 1997: Potential vorticity, easterly waves, and tropical cyclogenesis. *Mon. Wea. Rev.,* **125,** 2699–2708.
——, D. Vollaro, S. Skubis, and M. Dickinson, 2000: Origins and mechanisms of eastern Pacific tropical cyclogenesis: A case study. *Mon. Wea. Rev.,* **128,** 125–139.
Nakazawa, T., 1986: Intraseasonal variations of OLR in the Tropics during the FGGE year. *J. Meteor. Soc. Japan,* **64,** 823–839.
Nitta, T., and Y. Takayabu, 1985: Global analysis of the lower tropospheric disturbances in the Tropics during the northern summer of the FGGE year. Part II: Regional characteristics of the disturbances. *Pure Appl. Geophys.,* **123,** 272–292.
Raymond, D. J., and D. J. Torres, 1998: Case-studies of developing east Pacific easterly waves. *Quart. J. Roy. Meteor. Soc.,* **124,** 2005–2034.
Reed, R. J., and E. E. Recker, 1971: Structure and properties of synoptic-scale wave disturbances in the equatorial western Pacific. *J. Atmos. Sci.,* **28,** 1117–1131.
——, A. Hollingsworth, W. A. Heckley, and F. Delsol, 1988: An evaluation of the performance of the ECMWF operational system in analyzing and forecasting easterly wave disturbances over Africa and the tropical Atlantic. *Mon. Wea. Rev.,* **116,** 824–865.
Ritchie, E. A., and G. J. Holland, 1999: Large-scale patterns associated with tropical cyclogenesis in the western Pacific. *Mon. Wea. Rev.,* **127,** 2027–2043.
Sobel, A. H., and C. S. Bretherton, 1999: Development of synoptic-scale disturbances over the summertime tropical northwest Pacific. *J. Atmos. Sci.,* **56,** 3106–3127.
——, and E. D. Maloney, 2000: Effect of ENSO and the MJO on western North Pacific tropical cyclones. *Geophys. Res. Lett.,* **27,** 1739–1742.
Sui, C.-H., and K.-M. Lau, 1992: Multiscale phenomena in the tropical atmosphere over the western Pacific. *Mon. Wea. Rev.,* **120,** 407–430.
Takayabu, Y. N., and M. Murakami, 1991: The structure of super cloud clusters observed in 1–20 June 1986 and their relationship to easterly waves. *J. Meteor. Soc. Japan,* **69,** 105–125.
——, and T. Nitta, 1993: 3–5 day-period disturbances coupled with convection over the tropical Pacific Ocean. *J. Meteor. Soc. Japan,* **71,** 221–245.
Thorpe, A. J., 1985: Diagnosis of balanced vortex structure using potential vorticity. *J. Atmos. Sci.,* **42,** 397–406.
Wheeler, M., and G. N. Kiladis, 1999: Convectively coupled equatorial waves: Analysis of clouds and temperature in the wavenumber-frequency domain. *J. Atmos. Sci.,* **56,** 374–399.
Yamazaki, N., and M. Murakami, 1989: An intraseasonal amplitude modulation of the short-term tropical disturbances over the western Pacific. *J. Meteor. Soc. Japan,* **67,** 791–807.